SUPPLEMENTARY INFORMATION

Hyperbolic Meta-Antennas Enable Full Control of Scattering and Absorption of Light

Nicolò Maccaferri[a,b¶*], *Yingqi Zhao*[a¶], *Tommi Isoniemi*[a], *Marzia Iarossi*[a,c], *Antonietta Parracino*[a], *Giuseppe Strangi*[a,d,e], *and Francesco De Angelis*[a*]

[a]Istituto Italiano di Tecnologia, Via Morego 30, 16163, Genova, Italy

[b]Present address: Physics and Materials Science Research Unit, Université du Luxembourg, L-1511 Luxembourg, Luxembourg

[c]DIBRIS, Università degli Studi di Genova, Via Balbi 5, 16126 Genova, Italy

[c]Department of Physics, Case Western Reserve University, 10600 Euclid Avenue, Cleveland, Ohio 44106, USA

[e]CNR-NANOTEC Istituto di Nanotecnologia and Department of Physics, University of Calabria, 87036, Italy

[¶]These authors contributed equally to this work.

Corresponding author: nicolo.maccaferri@uni.lu; francesco.deangelis@iit.it

Supplementary note 1: calculation of the effective dielectric constant of a multilayered metal/dielectric structures.

The dielectric constant of a hyperbolic metamaterial made of alternating layers of Au and dielectric material was calculated using an effective medium approximation. The effective dielectric constant for the multilayered bulk HMM along the two principal directions, namely the x-y plane and z-direction, is calculated as follows

$$\varepsilon_{x,y} = \frac{t_m \varepsilon_m + t_d \varepsilon_d}{t_m + t_d}$$

$$\varepsilon_z = \frac{\varepsilon_m \varepsilon_d (t_m + t_d)}{t_d \varepsilon_m + t_m \varepsilon_d}$$

where t_m and t_d are the thicknesses of Au and the dieletric, respectively, and ε_m is the dielectric constant of Au, while ε_d is a dielectric constant of the dielectric layer. In Supplementary Figure S3 we plot, as a function of the wavelength of the incident light, the real part of the in-plane (x, y directions, blue curve) and out-of-plane (z direction, violet curve) components of the dielectric tensor. It is worth noticing that the hyperbolic regime is crucial to display two well separated decay channels. As reported in Supplementary Figure S3, when the structure has a dimension such that its supported resonances are no more in the hyperbolic region, the absorption peak due to the magnetic dipolar resonance is no more present, while it is present only the usual peak related to the electric dipole resonance. A similar behavior was also proved experimentally by Yang et al. [1]. Importantly, to be noticed in the top-panel of Supplementary Figure S1, the in-plane effective permittivity of a HMM is quite different from that of pure gold, showing that a change of the effective free electron density is made possible in hyperbolic metamaterials along the conductive plane. The effective

refractive index can be modified also by the selection of metal and dielectric and their relative shares in the multilayer.

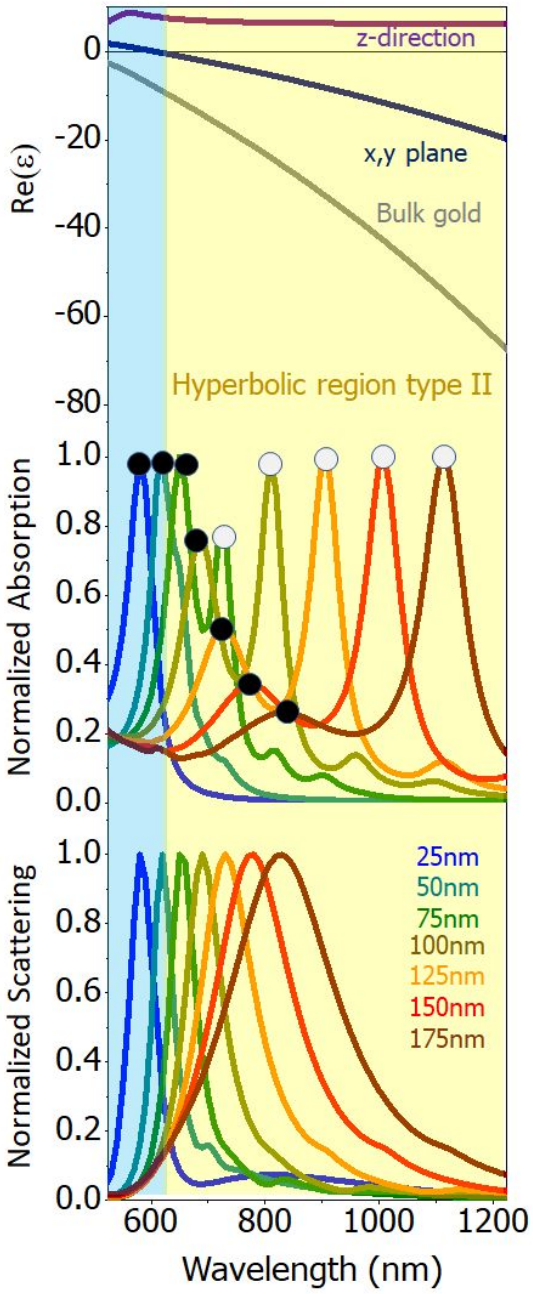

Supplementary Figure S1. Top panel: real part of the dielectric function of a HMM of type II made of multilayers of Au (10 nm each) and of a dielectric material (20 nm each) with n = 1.5 calculated using the effective medium theory (z-direction component – violet curve; x-y plane component – blue curve. The grey line is the real part of the dielectric function of bulk gold.

Normalized absorption (middle panel) and scattering (bottom panel) cross section for meta-antennas made of five bilayers of Au (10 nm each) and of a dielectric material (20 nm each) with n = 1.5 and with different diameters.

Supplementary note 2: optimization of the hyperbolic meta-antennas dimensions and composition.

We have performed an optimization study to find the best configuration, in terms of layers thicknesses and meta-antenna diameter, to maximize the spectral separation between scattering and absorption channels. In Supplementary FigureS1a we plot the absorption cross section for 4 different cases: from the top to the bottom we plot the absorption cross sectionfor Au thickness ranging from 10 nm to 40 nm, as a function of the wavelength of the incoming light and of the dielectric layer (n = 1.5) thickness, whose range is comprised between 10 nm and 40 nm. In Supplementary Figure S1bwe plot the scattering cross section, indicating with a green line the position of the absorption band resonant peak. The best configuration has been found to be that where the gold thickness is 10 nm and the dielectric thickness is 20 nm.

We have also studied what is the dependence of scattering and absorption cross sections on the meta-antenna diameter. In Supplementary Figure S2 we plot the absorption (top-panel) and scattering (bottom-panel) cross sections as a function of the wavelength of the incoming radiation and of the antenna radius. Au and dielectric (n = 1.5) are assumed to have a thickness of 10 nm and 20 nm, respectively. For diameters below 300 nm we have a clear separation between scattering and absorption bands.

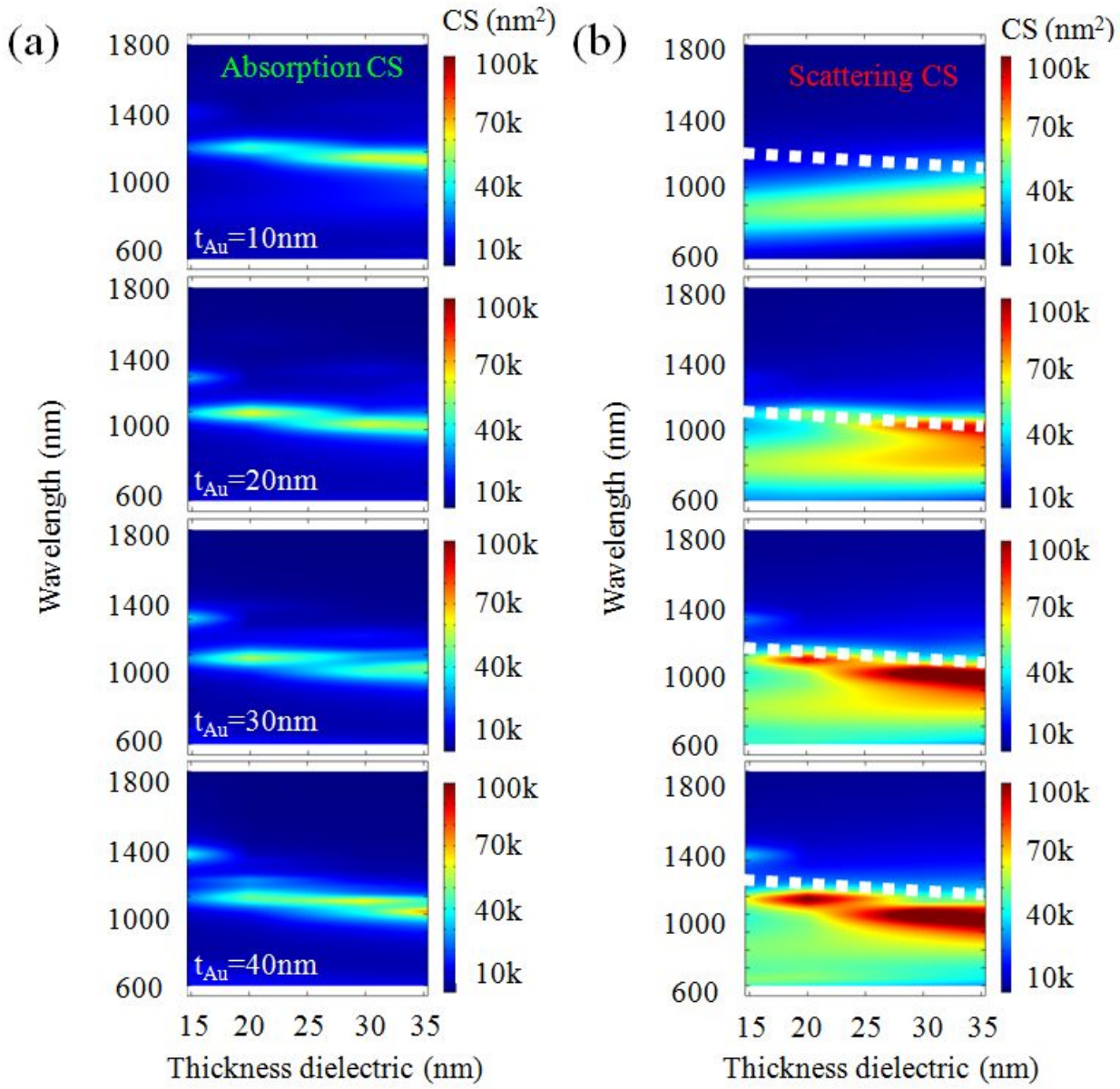

Supplementary Figure S2. (a) Absorption and (b) scattering cross sections of a hyperbolic meta-antenna on a glass substrate, with diameter 200 nm and made of five bilayers of Au and a dielectric with n = 1.5 as a function of the dielectric thickness, which varies from 10 nm to 40 nm, for Au thicknesses varying from 10 nm to 40 nm from the top to the bottom. The green line in (b) highlights the spectral position of the maximum of the absorption cross section plotted in (a).

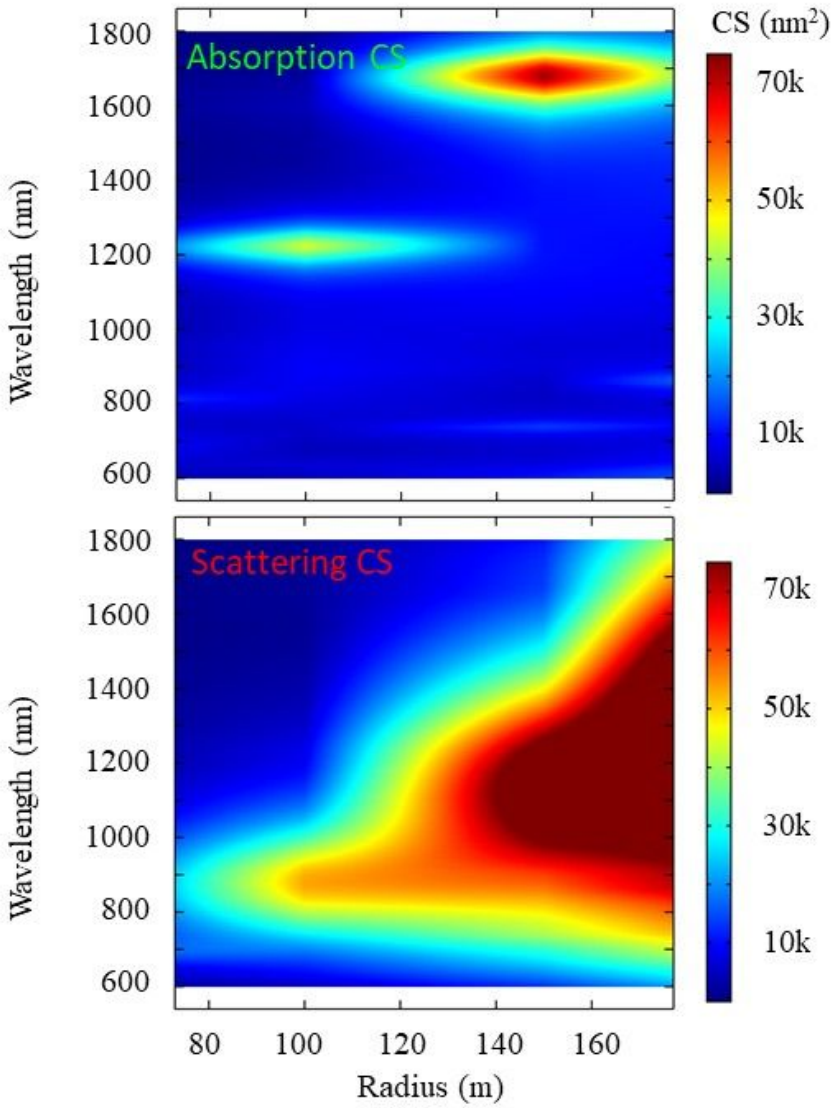

Supplementary Figure S3. Absorption (top) and scattering (bottom) cross sections of a hyperbolic meta-antenna on a glass substrate, made of five bilayers of Au (10 nm each) and a dielectric (20 nm each) with n = 1.5 as a function of the meta-antenna radius, which is varied from 75 nm to 200 nm.

Supplementary note 3: dependence of the optical properties of the hyperbolic meta-antennas on the shape – the conical and square shape cases.

As briefly discussed in the main text, we studied also the dependence on the optical properties on the shape of the meta-antennas. In Supplementary Figure S4a we plot the absorption and scattering cross section for a conically-shaped meta-antenna on a glass substrate with different aspect ratio (AR – ratio between the bottom and top diameter) values. As it can be inferred by looking at this figure, it is clear that for AR < 0.5, there is an overlapping between the scattering and absorption decay channels. Moreover, if instead of a cylinder we consider a square-like pillar (the length of the square side is equal to the diameter of the cylinder, namely 200nm), the optical response does not change (see Supplementary Figure S4b, where we compare the scattering and absorption cross sections of a circular and a squared cylinder on a glass substrate).

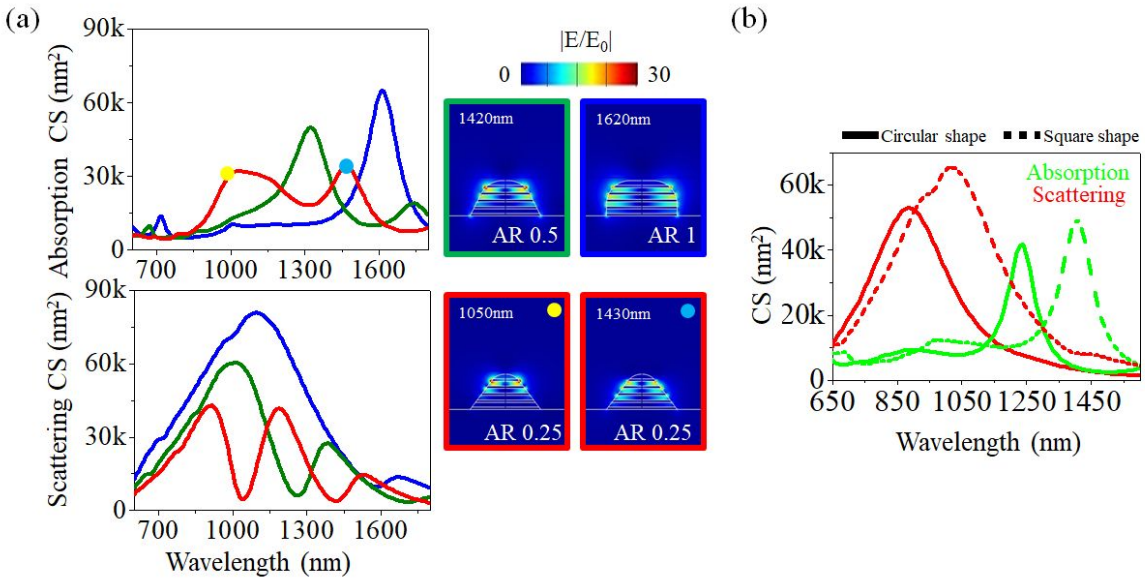

Supplementary Figure S4. (a) Absorption and scattering cross section (left-panels) for conical pillars with different AR. Near-field distribution of hyperbolic meta-antenna on a glass substrate in air at normal incidence and at the resonant wavelengths. (b) Absorption (green curves) and scattering (red curves) cross section of hyperbolic meta-antennas on a glass substrate in air at normal incidence for squared (dotted lines) and circular (continuous lines) shape.

Supplementary note 4: effect of the index contrast between the environment and the dielectric material composing the meta-antenna

To display two well-separated channels of almost pure scattering and absorption, it is crucial to have also an index mismatch between the dielectric material in the hyperbolic meta-antenna and the external environment. As shown in the main manuscript, due to the strong index mismatch, at the magnetic dipole-induced resonance (absorption peak) the electric and magnetic fields are almost totally localized within the meta-antenna, giving rise to strong absorption and to negligible scattering. On the contrary, if we assume that our system is immersed in a homogenous medium with the same index as the dielectric material (in this case n = 1.5, see also Supplementary Figure S5), we can observe a huge increasing of the scattering at the magnetic dipole-induced resonance (see the peak of the red curve at 1300 nm in the top-right panel of Supplementary Figure S5). In this case we can observe that at 1300 nm the magnetic near-field (middle-right panel of Supplementary Figure S5), is still concentrated inside the meta-antenna but there is also a not negligible component outside it. In this case there is not a strong index mismatch between the environment and the dielectric composing the meta-antenna. The index matching between the dielectric composing the nanostructure and the external environment induces a strong quenching of the currents in the bottom side of the meta-antenna. Indeed, we can observe a strong far-field emission (see the bottom-right panel in Supplementary Figure S5), which has the same intensity of the electric dipole resonance-induced far-field pattern plotted in the bottom-left panel of Supplementary Figure S5.

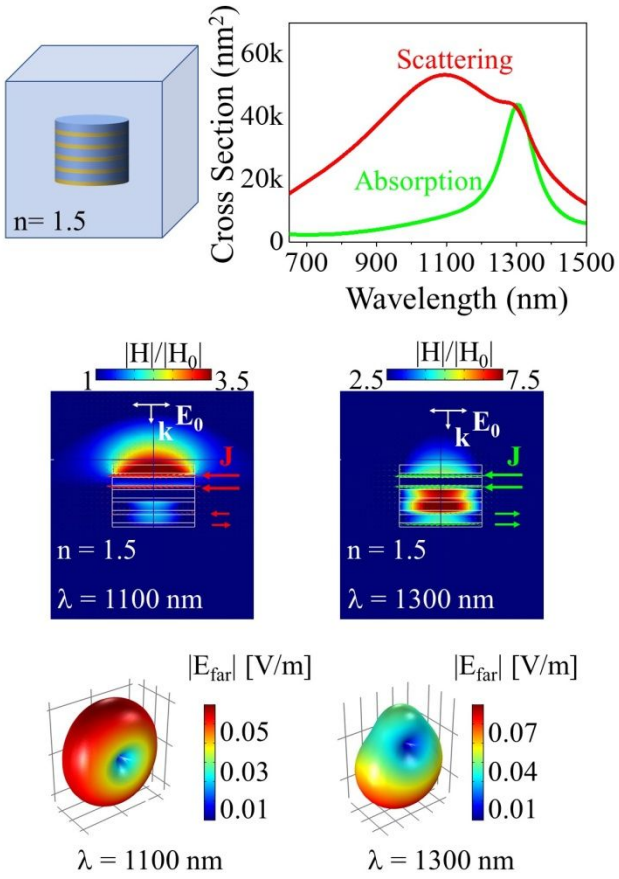

Supplementary Figure S5. Top-left panel: sketch of a hyperbolic meta-antenna with D = 250 nm and made of five bilayers Au (10 nm each) and a dielectric material with n = 1.5 (20 nm each) immersed in a homogeneous transparent and non-conductive medium with n = 1.5. Top-right panel: related scattering and absorption cross section as a function of the wavelength of the incoming light. Middle-panel: magnetic near-field distribution at 1100 nm (left panel) and at 1300 nm (right panel). The red and green arrows indicate the direction of the current density J inside the metallic layers. Bottom-panel: electric far-field distribution at 1100 nm (left panel) and at 1300 nm (right panel).

Supplementary note 5: dependence of the optical properties of the hyperbolic meta-antennas on the number of the metal/dielectric layers.

A desired control of both $\sigma_{scat}/\sigma_{abs}$ and $\sigma_{abs}/\sigma_{scat}$ is possible by changing the number of the Au/dielectric layers in the meta-antenna, starting from one bilayer (plasmonic gold nanoantenna 10 nm thick with a capping layer of dielectric with n = 1.5 and 20 nm thick) up to 8 bilayers. The diameter of the meta-antennas is equal to 200 nm and the structures are assumed to lie on glass substrate. As it can be inferred from both the near-field plots (top-panel of Supplementary Figure S6), which were calculated at the resonant wavelengths, i.e. where the absorption is maximum, and the absorption curves, up to 3 bilayers – antenna, MIM and metal-insulator-metal-insulator-metal (MIMIM) structures – we do not observe any absorption peak in addition to the one due to the electric dipole-induced LSPR excited throughout the structure. Starting from the 4 bilayers case we can observe at larger wavelengths (around 1300 nm) the rising of an almost pure absorption band due to the excitation of a magnetic dipole within the meta-antenna. It is important noticing that a strong near-field confinement and intensity enhancement (> 300, a factor 3 with respect to the MIMIM case) is observed at the wavelength where the magnetic dipole-induced absorption band is maximum. Moreover, as it can be inferred from the central cases of four, five and six bilayers, we can actually control either the spectral position where $\sigma_{scat} = \sigma_{abs}$ or the relative intensity between the two maxima of $\sigma_{scat}/\sigma_{abs}$ and $\sigma_{abs}/\sigma_{scat}$ by changing the number of layers. We can pass from a situation where $\sigma_{abs}/\sigma_{scat}$ is higher than $\sigma_{scat}/\sigma_{abs}$ (4 bilayers case) to a case where they are equal (five bilayers case), to finally arrive to a case where $\sigma_{abs}/\sigma_{scat}<\sigma_{scat}/\sigma_{abs}$. As can be seen from Supplementary Figure S6, the best configuration to obtain two distinct and totally de-coupled scattering and absorption bands, namely an almost pure scattering and an almost pure absorption bands with the same efficiency/intensity, is the configuration with five bilayers, that is the architecture presented in this work. If we have 6 or more bilayers we start to see a second peak in the scattering cross section at the same wavelength of the magnetic dipole-induced absorption peak,

giving rise to a quenching of $\sigma_{abs}/\sigma_{scat}$, which becomes very much smaller than $\sigma_{scat}/\sigma_{abs}$ for $n_{bi\text{-}layers} > 5$. The second scattering band appearing already in the 6 bilayers case reaches almost the same intensity of the magnetic dipole-induced absorption band once we reach the 8 bilayers case. Regarding the main scattering peak present in all the systems considered, from the classical planar plasmonic antenna up to the 8 bilayers hyperbolic meta-antenna, the far-field pattern is the one we expect from a dipolar antenna, as it is actually related to the excitation of an electric dipolar mode. Finally, for completeness, we plot also the far-field distributions of the 6, 7 and 8 bilayers cases at the magnetic-dipole induced absorption resonant wavelength (see Supplementary Figure S7). In this case we can observe a strong forward and backward scattering, in contract with the more uniform far-field distribution observed at the electric dipole-induced scattering peak.

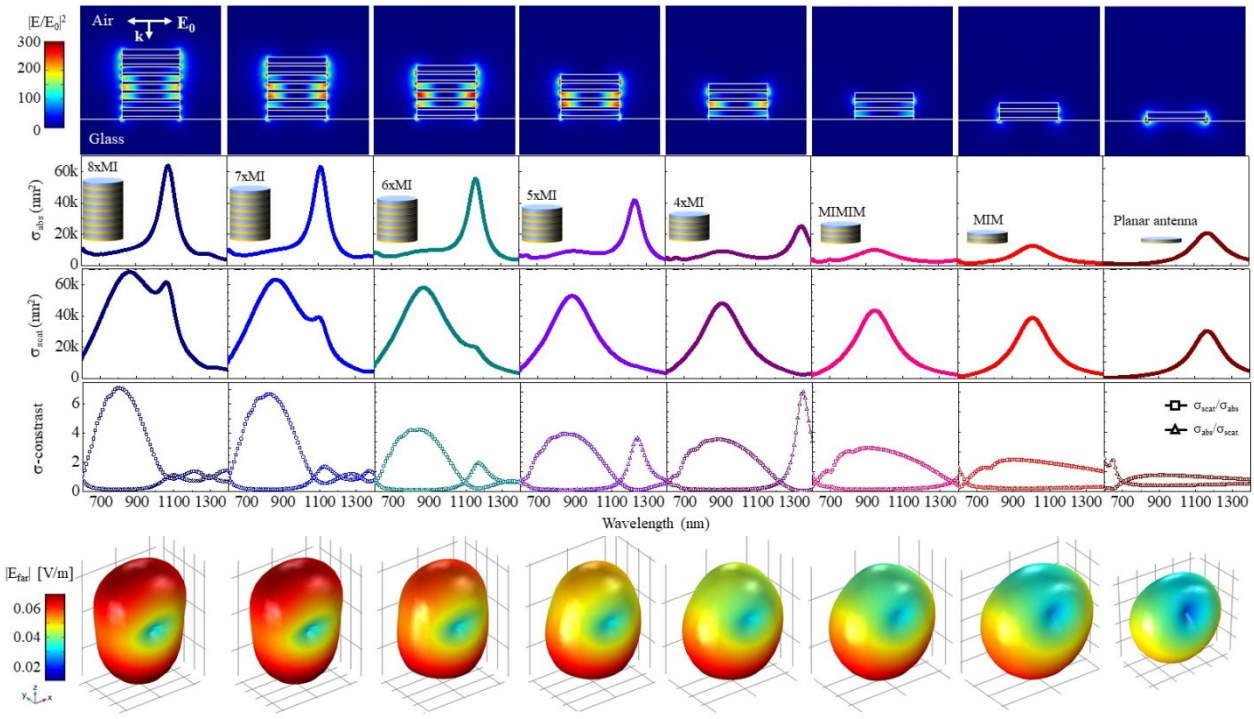

Supplementary Figure S6. Top-panel: Near-field intensity distribution of a hyperbolic meta-antenna on a glass substrate in air at normal incidence and at the resonant wavelength of the magnetic dipole-induced absorption band. Middle-panel: absorption (top), scattering (middle) and A and S (bottom panel) evolution upon variation of the number of bilayers. Bottom-panel: far-field distribution at the resonant wavelength of the electric dipole-induced scattering band.

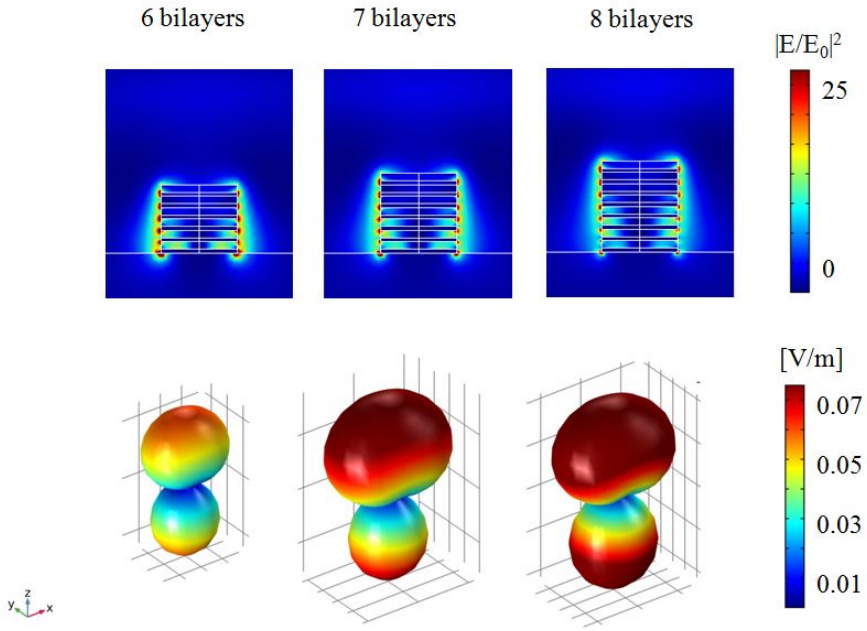

Supplementary Figure S7. Top-panel: Near-field distribution at the wavelengths of the scattering peak for the cases of 6, 7 and 8 bilayers presented in Supplementary Figure S6. Bottom- panel Far-field distribution at the wavelength of the absorption peaks for the cases of six, seven and eight bilayers presented in Supplementary Figure S6.

Supplementary note 6: dependence of the cross-section ratios on the direction and polarization of the incident radiation.

If we consider a random orientation of the meta-antenna in a homogenous medium, it can be shown that the overall response is that shown for a meta-antenna on a glass substrate with a clear separation between the scattering and absorption channels. In Figure S8 we plot $\sigma_{abs}/\sigma_{scat}$ and $\sigma_{scat}/\sigma_{abs}$ of a randomly oriented hyperbolic meta-antenna made of five bilayers of Au (10 nm each) and SiO_2 (20 nm each) in water (n = 1.33), demonstrating that the separation between the two channels is maintained also for systems randomly dispersed in a solvent.

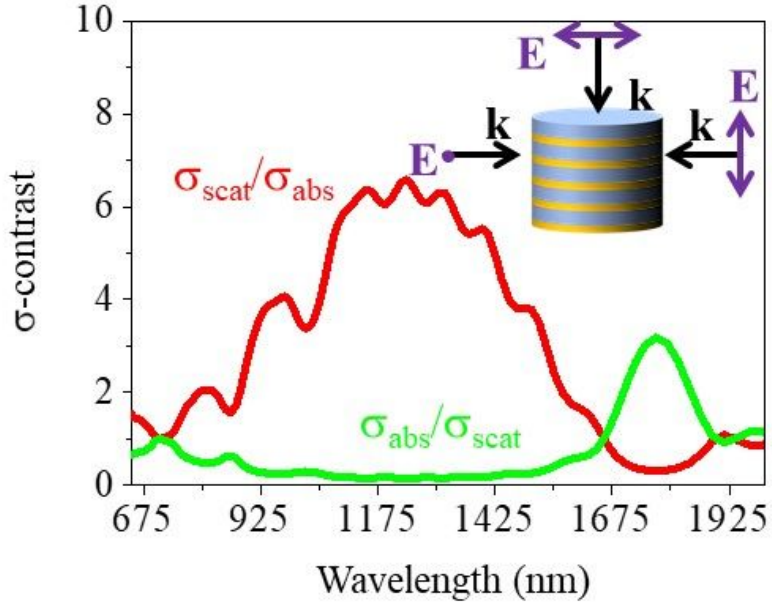

Figure S8. Calculated $\sigma_{scat}/\sigma_{abs}$ (red curve) and $\sigma_{abs}/\sigma_{scat}$ (green curve) of a randomly oriented hyperbolic meta-antenna made of five bilayers of Au (10 nm each) and SiO_2 (20 nm each) in water (n = 1.33). The curves are obtained by making a convolution of the cross sections obtained for the three different orientations between the incident electric field and the meta-antenna as shown in the inset.

[1] Yang, X.; Yao, J.; Rho, J.; Yin X.; Zhang X. *Nat. Photon.* **2012**, *6*, 450–454.